Fermilab Library
0 1160 0033759 4

STRASBOURG

CRN 93-52

FERMILAB
APR 7 1994
LIBRARY

Ta, Au and Th L X-Ray energy shifts induced by 0.6, 1.2, 2.4 and 4 MeV/nucleon Kr ions

J. Larcher*, C. Heitz*, G.J. Costa*, Y. El Masri**
J.M. Ferté**, F. Hanappe*** and P. Duhamel***

* Centre de Recherches Nucléaires et Université Louis Pasteur, Strasbourg, France
** Fond National de la Recherche Scientifique et Université Catholique de Louvain, Louvain-La-Neuve, Belgium
*** Fond National de la Recherche Scientifique et Université Libre de Bruxelles, Brussels, Belgium

CENTRE DE RECHERCHES NUCLEAIRES

STRASBOURG

IN2P3 UNIVERSITE
CNRS LOUIS PASTEUR

Ta, Au and Th L X-Ray energy shifts induced by 0.6, 1.2, 2.4 and 4 MeV/nucleon Kr ions.

J. Larcher*, C. Heitz*, G.J. Costa*, Y. El Masri, J.M.Ferté**, F. Hanappe*** and P. Duhamel*****

* Centre de Recherches Nucléaires et Université Louis Pasteur, Strasbourg, France
** Fond National de la Recherche Scientifique et Université Catholique de Louvain, Louvain -la -Neuve, Belgium
***Fond National de la Recherche Scientifique et Université Libre de Bruxelles, Brussels, Belgium

Abstract

The L X-ray spectra of Ta, Au and Th induced by 0.6 to 4 MeV/nucleon Kr beams have been studied by means of a LiF(100) equiped crystal spectrometer having an overall resolution of 30 eV at 8.146 keV. The energy shifts of the main lines have been measured with accuracies ranging from 5 eV for well separated lines, to 30 eV for poorly resolved lines. From the energy shifts vacancy configurations are deduced and compared to predictions of various theoretical models.

PACS : 32.30.Rj; 32.70.Jz; 34.50.Fa

I. Introduction

In early experiments concerned with heavy ion induced X-ray emission, characteristic line shifts and broadening have been observed and interpreted as the result of satellite production through multiple inner shell ionization [1]. The presence of spectator vacancies during an X-ray transition yields a change in the binding energies of the electron levels implied in the transition and consequently a shift of the corresponding X-ray energy. The broadening results from the overlapping of several satellite lines when the resolution of the detection system is insufficient to resolve them in individual lines. As a consequence, experiments concerned with multiple ionization range roughly into two categories :

i) High resolution measurements for resolved K and L satellites with energies below 10 keV : Most of these experiments are concerned with light elements in the range of $8<Z<30$ and present a marked tendency towards studies of chemical effects[2]. Recently a break-through has been realized in this field by Perny et al.[3] in a detailed study of the $K\alpha$ satellites of Mo (17 to 18 keV) induced by He and O ions. In all these experiments the electron vacancy configuration leading to the observed satellite spectra can be estimated in a relatively easy and unambiguous manner.

ii) Measurements with Si(Li) or Ge detectors yielding the energy shifts of characteristic peak centroids or changes in intensity ratios : From these measurements only an "average" or a "most probable" vacancy configuration can be deduced. This is especially the case for the L X-rays of heavy elements ($Z>50$) even when high resolution spectrometers are used. Whereas for the K satellites of light elements ($Z<20$) the contributions of transitions implying outer shell vacancies are inexistent or negligible, this is not longer the case for the L satellites of heavy elements ($Z>70$) for which N, O and P levels are occupied. Here the numerous satellites resulting from the different vacancy distributions produce again a broadening of the X-ray lines and the shifts of their centroids.

Nevertheless the study of heavy ion induced L X-ray spectra of heavy elements with high resolution equipements will present some advantages. As a consequence of the better energy resolution of these instruments the deconvolution of the spectra is easier and of course more accurate than for Si(Li) spectra. This results in a better definition of the peak centroids especially in the case of overlapping lines. Generally speaking, energy shifts can be calculated with a better accuracy thus allowing more definite comparisons with theoretical predictions.

The choice of the Kr - Ta, Au, Th collision systems results from the consideration of the relative binding energies of the projectile K and the target L levels [4]. Owing to the Molecular Orbital (MO) ionization mechanism and especially to the $3d\sigma$ vacancy sharing between the projectile K and the target L levels [5], the L levels of Ta and Au can be easely excited whereas those of Th are less affected. As a consequence some differences are expected between the results for Ta and Au and those for Th.

II. Experimental procedure

Experiments have been performed at the Isochronous Cyclotron of Louvain-la-Neuve (Belgium) with Kr ion beams of 0.6, 1.2, 2.4 and 4 MeV/nucleon. The corresponding charge states have been 8+, 13+, 13+ and 17+ respectively. A schematical view of the equipment is shown in figure 1. The target chamber is electrically isolated thus allowing charge integration and consequently an automatical monitoring of the angular displacements of the analyzing crystal and of the detector. The thick Ta, Au and Th targets were disposed on an air cooled target holder and positioned at 45° with respect to the beam direction. The emitted X-rays were analyzed perpendicularly to the beam axis, by a planar 100 LiF crystal and detected by a 1 mm thick INa(Tl) scintillation detector. Soller slits are situated between the target and the crystal and between the latter and the detector. All alinements of slits, crystal and detector have been performed with ^{55}Fe and ^{57}Co sources. Furthermore for the Ta and Th targets, a run with a 4 MeV proton beam has been achieved in order to check the energy calibration and the resolution of the equipment. The X-ray energy tables of Bearden [6] have been used throughout the whole experiment. The monodimensional spectra (number of events as a function of the angular position of the detector) were recorded in a multiscaling mode for a given amount of charges on the target. The complete process, including the crystal and detector motions, was computer controlled using a CAMAC interface. As an example, figure 2 shows the Ta $L\beta$ spectra induced by 2.4 MeV/nucleon Kr ions and by 4 MeV protons. Under the present conditions the FWHM of the $L\alpha_1$ lines of Ta (8.146 keV) and of Th (12.969 keV) were 30 eV and 100 eV respectively.

In the case of Ta and Au targets, the 2Θ angular steps of the detector were 0.04°, whereas 0.02° steps were used for the Th target, corresponding to 6 eV and 9 eV energy steps respectively for the previously indicated lines. Owing to the loss of efficiency of this detection system in regard of the efficiency of common solid state detectors, the acquisition times were considerably increased and ranged from 6 to 9 hours per spectrum. The use of thin targets would result in prohibitif acquisition times. As a consequence the spectra obtained for the nominal beam energies contain non negligible contributions from slown down Kr ions. However these contributions are not excessive essentially because self absorption of the produced X-rays is relatively high and because their production cross section drops steeply with decreasing ion energy.

III. Results and discussion

The X-ray spectra obtained for the three elements at the various bombarding energies are shown in figures 3, 4 and 5 . All spectra are normalized for 3.5×10^{12} impinging Kr ions. The measured X-ray energies and the corresponding energy shifts of the different L lines are listed in Table 1. The accuracies of the measurements are the following :

- For isolated and well defined lines *e.g.* L*l* or Lα lines : 5 eV.
- For proeminent lines *e.g.* Lβ_1, Lγ_1 and Lβ_2 : 10 eV
- For low intensity lines which have to be extracted from complex peaks *e.g.* Lβ_3, Lβ_4 and L$\gamma_{2,3}$ or L$\gamma_{4',4}$: 30 eV.

Concerning the spectra the following comments can be made:

a) Ta spectra.

All lines observed in proton bombardment are present in the Kr induced spectra but shifted and broadened as expected. Only the low intensity Lη line cannot be observed as a consequence of the broadening and overlapping of the high energy tail of the shifted Lα peak. At the highest energies (2.4 and 4 MeV/nucleon) the L$\gamma_{4',4}$ lines merge under the Kr-Kα line. The intensity of The Kr-K lines increases as a function of the projectile energy. This is in concordance with the 3dσ vacancy sharing process between the Kr-K and the Ta-L levels [5]. The striking effect is the appearance of the main L diagram lines of Ta ((L*l*)^0, (Lα_1)^0, (Lβ_1)^0 and (Lγ_1)^0) at bombarding energies above 1.2 MeV/nucleon (Figure 6). The intensity of these lines increases with increasing beam energy.

b) Au spectra.

The Au and Ta spectra present the same features. The main difference is due to the presence of the projectile K lines near the target Lβ and Lγ lines. Especially the matching of the Kr - Kβ and the Au - Lγ lines presents some difficulties for the deconvolution and the attribution of the latter.

c) Th spectra.

These spectra present some important differences with the former :

i) The Kr - K lines are relatively more intense indicating that through the MO ionization essentially the projectile K level is excited [4]. Especially for 0.6 MeV/nucleon ions only target X-rays corresponding to the L_3 level are visible. In this case the 3dσ vacancy sharing is limited to the Kr -K and the Th - L_3 levels. For the higher bombarding energies the three L levels are excited.

ii) Only at the highest bombarding energy the (L*l*)^0 and (Lγ_1)^0 diagram lines can be observed (Figure 7). It may be assumed that the (Lα_1)^0 and the (Lβ_1)^0 lines are also present

but can not be identified as a consequence of the matching of the intense Kr - Kα and the Th Lα peaks, and the complexity of the Lβ system respectively. Nevertheless and especially for the Lα lines an accurate deconvolution of the spectrum can only be achieved by taking in account the $(L\alpha_1)^0$ and $(L\alpha_2)^0$ diagram lines (Figure 8).

Several processes can be invoked to explain the presence of diagram lines :

- Ionization by secondary electrons : The energy transfer of 0.6 to 4 MeV/nucleon Kr ions to a free electron varies from 1.3 to 8.8 keV. For bound electrons the transfer may be substantially higher but the production cross section of these electrons drops with increasing energies [7], so that this contribution is probably negligible.

- The photoionization by shifted intense X-radiations as proposed by Schleinkofer et *al.*[8] can also be invoked mainly in the case of Ta : here as soon 0.6 MeV/nucleon the energy of the shifted $L\beta_2$ line (9.935 keV) is higher than the L_3 absorption edge (9.877 keV) so that all corresponding lines may be excited. A rather more important contribution may arise from photoionization by the K X-rays of the projectile (12.7 to 15 keV) the energies of which are higher than the three L absorption edges of Ta and the intensities of which are of the same order of magnitude than the Ta $L\beta_2$ rays. Unfortunately the same mechanism cannot explain the production of the diagram lines in Au and Th so that it becomes doubtfull that it works only for Ta.

- Photoionization by target K lines.

- Internal conversion of nuclear transition energies resulting from Coulomb excitation.

It will be shown that the two last effects are the most efficient processes for the production of diagram lines in these collision systems(to be published).

The most interesting observations in the present experiments concern the energy shifts of the peak centroids listed in Table 1. First it is obvious that for the same groups of transitions (that is, LM or LN transitions) the shifts are not equal but of the same order of magnitude. This appears clearly in figure 9 concerning the Ll (L_3M_1) and the Lα $(L_3M_{4,5})$ shifts of Ta. From figure 9 it is also obvious that the shifts vary linearly with the beam velocity. This allows us to determine some shifts by extrapolation for further use in the cases where the lines cannot be extracted from the spectra. Table 1 indicates also the velocity U of the Kr ions expressed in atomic units (1 a.u. = cα = 0.219 x 10^9 cm/s).

The coefficients a and b corresponding to the linear evolution E(keV) = a + bU(a.u.) of the energy shifts as a function of the ion velocity U, and the linear regression coefficient r^2 are indicated in Table 2 for the various lines. For a given bombarding energy, the shifts decrease linearly with increasing target Z as shown in figure 10.

It is well known that the energy shifts of the characteristic X-ray lines result from supplementary spectator vacancies during the radiative transition. To determine these vacancy configurations one has to use known theoretical (or experimental) energy shifts induced by defined vacancies and to estimate the number of vacancies in accordance with the observed experimental shift. This has to be done for each observed line and, of course,

the same configuration must account for the shifts of all lines. Several autors report theoretical values either of mean energy shifts per vacancy or shifts for a defined vacancy or vacancy configuration [9 to 16]. For M vacancies interesting values for the present discussion are represented in figure 11. The values deduced from the calculation of Zschornak *et al.* [15] are much higher than those reported by the other authors probably because the model supposes the prior stripping of all outer electrons down to the M shell.

From the present measurements it appears first that spectator L vacancies are not frequent : Indeed if we assume that the number of M and N vacancies will increase with the ion energy and that at the highest impact energy a L_3 spectator vacancy is present this would induce an approximate energy shift of the Ta Lα line of 154 eV [9] leaving 214 - 154 = 60 eV for the effect of M and N vacancies. If we consider only the contribution of the former with a shift of 29 eV per $M_{4,5}$ vacancy[9], we calculate two $M_{4,5}$ vacancies. Looking at the lower impact energies (0.6 and 1.2 MeV/nucleon) we observe that the shifts (84 and 118 eV respectively) are lower than the one resulting from an L spectator vacancy. So the shift must be attributed to M vacancies and, neglecting N vacancies, we calculate an approximate number of 3 for 0.6 MeV/nucleon ions and 4 for 1.2 MeV/nucleon ions.These numbers are higher than the one obtained for the higher bombarding energy when an L spectator vacancy is assumed. As a consequence the higher shift at the higher ion energy must be acounted for by a larger number of M and N vacancies and not by a supplementary L vacancy. As a conclusion, in the case of Ta, we can rule out contributions from supplementary L vacancies and interprete the measured shifts by M and N vacancies. This is also the case *a fortiori* for Au and Th targets. Only the high energy end of the shifted peaks may account for an L spectator vacancy.

The problem is now the choice of the shifts induced per M and N vacancies. The use of the values calculated according to the model of Burch *et al.* [9] does not yield concordant vacancy configurations for the different lines. The same effect occurs when mean energy shifts from Hagmann [10] or Uchai *et al.* [14] are used. This indicates that the measurements are accurate enough to reveal the small energy differences between shifts for supplementary M vacancies. Indeed as pointed out by Hagmann [10] and as it appears in the calculations of Uchai *et al.*[14] and Zschornak *et al.*[15] the shift per M vacancy increases with the number of M vacancies still present at the moment of the electron transition. For example in reference [14] the shifts for the Ta Lα line vary from 21 eV for the first M vacancy, to 27 eV for the eleventh whereas the mean value is 23.8 eV.Thus the best concordance between the vacancy configuration and the Measured energy shifts for the different lines is found with the values of Uchai for increasing numbers of M vacancies. The use of these values implies implicitly that the M spectator vacancies begin to appear in the M_5 level. Such an hypothesis is not unfounded because through Coster - Kronig transitions deeper M vacancies may be transferred to the M_5 level befor the occurence of a

radiative transition. The calculations are illustrated in tables 3, 4 and 5 resuming the estimation of the number of M and N vacancies in Kr - Ta, Au and Th collisions. In reference [14] neither shifts for $L\beta_2$ nor those for supplementary N vacancies are calculated. Hagmann [10] using the DFS code of Fricke [16], reports for the $L\alpha$ and the $L\beta_2$ lines and elements ranging from Yb to Th, 6 eV and 19 eV per N vacancy respectively. Rao et al. [12] reports values of 2 - 4 eV per N vacancy for the $L\alpha$ lines of Yb, W and Pt, and 5 - 9 eV, 6 - 11 eV and 8 - 13 eV per N vacancy for the $L\gamma_1$ lines of the same elements respectively. As the $L\beta_2$ line corresponds to an L_3N_5 transition we can assume that the energy shift per M vacancy is of the same order of magnitude than the one corresponding to other LN transitions and especially must be close to the shift of the $L\gamma_1$ line (L_2N_4 transition). So to estimate the shift $\Delta L\beta_2$ we use the values $\Delta L\gamma_1$ of Uchai *et al.*[20] and multiply them by the experimental ratio $\Delta L\beta_2 / \Delta L\gamma_1$. This procedure gives us the shifts resulting from M vacancies of the $L\beta_2$ lines for Ta, Au and Th as indicated in tables 3, 4 and 5. The same procedure will be used for the $L\beta_3$ and $L\beta_4$ lines for which the values of the shifts of the $L\beta_1$ line from [14] are adopted to start the calculation. Mean energy shifts per M vacancy for the $L\beta_2$ lines of Ta, Au and Th deduced from these values are the following : 60, 66 and 79 eV respectively. These values are somewhat lower than those reported by Hagmann [10] (78, 84 and 91 eV respectively). Of course, owing to the different basical assumptions of the theoretical models, they are much lower than the values calculated through the initial model of Burch [9] : 89, 99 and 118 eV respectively. The mean shifts per M vacancy of the $L\beta_2$, $L\beta_3$ and $L\beta_4$ lines are listed in table 6. Values of mean energy shifts of the $L\beta_3$ and $L\beta_4$ deduced from the calculations of Zschornak *et al.*[15] have been calculated assuming 6 vacancies in the M5 subshell. The corresponding shifts for the $L\beta_2$ line cannot be calculated.

Shifted $L\gamma_2$ and $L\gamma_3$ lines can not be resolved. As a consequence, to calculate the energy shifts, the mean energies of the diagram lines have been used in table 1. For the estimation of the vacancy configuration in tables 3 to 5 the mean values of the energy shifts for the $L\gamma_2$ and $L\gamma_3$ lines from Uchai *et al.*[14] have been used. The same procedure has been employed for the $L\gamma_{4'}$ and $L\gamma_4$ lines.

Concerning the energy shifts induced by N spectator vacancies the evaluation is more difficult essentially because inacuracies from experiment and theory add up and become of the same order of magnitude than the expected shifts per N vacancy. Nevertheless starting from values of Hagmann [10] which seem to be the more realistic and are of the same order of magnitude than those reported by Rao *et al.* [12], we can calculate an approximate number of N vacancies by dividing the difference between a defined experimental shift and the theoretical shift from Uchai *et al.* [14] induced by M vacancies, by the mean shift per N

vacancy of the of the same line. To determine these values we start our calculations with shifts of the order of 6 eV for the $L\alpha$ lines and 20 eV for the $L\beta_2$ lines taken from [10]. This procedure may introduce some errors of the order of some eV for the highest numbers of vacancies and for the largest energy shifts. The results of this estimation are given in table 7 and used in tables 3, 4 and 5 to calculate the various electron configurations. The remaining rest of energy shifts is attributed to O and outer spectator vacancies and to the errors at the various stages of the calculations. We observe that only for the Au $L\beta_1$ line (Table 4) negative values appear in the column "rest" indicating that the measured shifts are probably too low. However the differences are within the experimental error (10 eV) for this line. Assuming that the number of O vacancies is probably somewhat lower than the one of N vacancies [17, 18] we can see that for the $L\alpha$ line the mean energy shift for an O vacancy is somewhat less than 1 eV. It is higher for LN transitions as it can be seen for the $L\gamma_1$ (L_2N_4) and $L\beta_2$ (L_3N_5) shifts in the tables. In table 8 are resumed the average vacancy configurations deduced from the present measurements. These configurations are comparable to those reported by other authors for collision systems having similar characteristics (ion energies and heavy targets) : Pepper *et al.*[20] indicate 3 to 4 M vacancies for 0.5 to 2.25 MeV/nucleon O ions impinging on Ce. Hagmann *et al.* [10, 21], for 6.3 to 47 MeV I projectiles incident on Yb, Au and Th, report 2 - 4, 1 - 4 and 1 - 2 M vacancies respectively and about 10 N vacancies for the same elements. For 88 MeV Ne ions incident on Bi Ito *et al.* [19] estimate the number of M vacancies to 2 and the one of N vacancies to 11. With 37.5 MeV Si ions and the same target Rao *et al.* [12] estimate the number of M vacancies to be at least 3. The most important discrepancy is concerned with values from Uchai *et al.* [18] who for 1 MeV/nucleon Ag ions incident on Au report very high numbers of spectator vacancies in the L, M and O shells : $n_M = 7$, $n_N = 20$ and $n_O = 7$. This distribution results from the underestimation of the energy shift of the $L\alpha$ line resulting from an N vacancy (0.5 eV) which is approximately a factor 10 less than commonly adopted values (6 eV).

IV. Conclusions

The use of a wavelength dispersive detection system undoubtedly gives more accurate measurements of the energy shifts resulting from multiple ionization in heavy ion induced X-ray emission. The present results give strong support to the theoretical calculations of Uchai *et al.*[14]. However, to get more insight into the complex satellite structures, very high resolution equipment is required especially in the case of the L X-rays of heavy elements. This will be a very difficult task mainly as a consequence of the large number of satellite lines resulting from the various N vacancies.

Acknowledgments

The authors are indebted to the operating crew of Louvain-la-Neuve Cyclotron for the excellent and efficient running of the machine. They wish also to thank CGRI (Belgium) and IN2P3 (France) for financial and administrative support.

References

1. Garcia, J.D., Fortner, R.J., Kavanagh, T.M.: Rev. Mod. Phys. **45**, 111 (1973)
2. Raman, S., Vane, C.R. : Nucl. Instr. and Meth. **B3**, 71 (1984)
3. Perny, B., Dousse, J.-Cl., Gasser, M., Kern, J., Rhême, Ch., Rymuza, P., Sujkowski, S. : Phys. Rev. A **36**, 2120 (1987)
4. Meyerhof, W.E., Anholt, R., Eichler, J., Salop, A. : Phys. Rev. A **17**, 108 (1978)
5. Heitz, Ch., Hagmann, S., Kraft, G., Kwadow, M. : J. Phys. B: Atom. Molec. Phys. **12**, 1851 (1979)
6. Bearden, J.A.: Rev. Mod. Phys. **39**, 78 (1967)
7. Mokler, P.H., Folkmann, F. : Topics in Current Physics Vol. **5**, Structure and Collisions of ions and atoms, Edited by I.A. Sellin, pp 201 - 271, Berlin, Heidelberg, NewYork : Springer Verlag 1978.
8. Schleinkofer, L., Bell, F., Spindler, E., Betz, H.D.: J. Phys. B: Atom. Molec. Phys. **11**, L451 (1978)
9. Burch, D., Wilets, L., Meyerhof, W.E. : Phys. Rev. A**9**, 1007 (1974)
10. Hagmann, S. : GSI - Bericht Pa - 1 - 77
11. Parente, F., Chen, M.H., Crasemann, B., Mark, H. : At. Data Nucl. Data Tables **26**, 383 (1981)
12. Rao, P.V., Albridge, R.G., Ramayya, A.V., Andrews, M.C., Mehta, R., McDaniel, F.D., Miller, P.D. : IEEE Trans. on Nucl. Sci. NS - **28**, 1112 (1981)
13. Roy, S.K., Ghosh, D.K., Talukdar, B. : Phys. Rev. A**28**, 1169 (1983)
14. Uchai, W., Nestor Jr., C.W., Raman, S., Vane, C.R. : At. Data Nucl. Data Tables **34**, 201 (1986)
15. Zschornak, G., Musiol, G., Wagner, W., Report ZfK-574 (1986) Rossendorf bei Dresden
16. Fricke, B. : Theor. Chim. Acta **21**, 235 (1971)
17. Parente, F., Carvalho, M.L., Salgueiro, L. : J. Phys. B : At. Mol. Phys. **16**, 4305 (1983)
18. Uchai, W., Lapicki, G., Milner, W.T., Raman, S., Rao, P.V., Vanes, C.R. : J. Phys. B : At. Mol. Phys. **18**, L389 (1985)
19. Ito, S., Shoji, M., Maeda, N., Katano, R., Mukoyama, T., Ono, R., Nakayama, Y. : J. Phys. B : At. Mol. Phys. **20**, L597 (1987)
20. Pepper, G.H., Lear,R.D., Gray, T.J., Chaturvedi, R.P., Moore, C.F. : Phys. Rev. **A12**, 1237 (1975)
21. Hagmann, S., Armbruster, P., Kraft, G., Mokler, P.H., Stein, H.J. : Z. Physik A **288**, 353 (1978)

Table 1 - Measured energies (E_X), energy shifts (ΔE_X) and calculated energy shifts ($\Delta' E_X$) of the main L lines of Ta, Au and Th as a function of the Kr ion energy (E_{Kr}) or velocity (U). Values with asterisks are extrapolated from the calculated values. The calculated energy shifts ($\Delta' E_X$) are deduced from the measurements assuming a linear variation $E_X = a + bU$ of the X-ray energy as a function of the ion velocity (Coefficients a and b are given in Table 2)

Line	Elem.	E_{Kr} (MeV/nucl)	0	0.6	1.2	2.4	4
		U (atomic units)	0	4.918	6.955	9.836	12.698
Ll	Ta	E_X (keV)	7.173	7.278	7.323	7.389	7.436
L_3M_1		ΔE_X (eV)	0	105	150	216	263
		$\Delta' E_X$(eV)	0	105	148	209	269
	Au	E_X (keV)	8.494	8.605	8.642	8.683	
		ΔE_X (eV)	0	111	148	189	
		$\Delta' E_X$(eV)	0	102	142	198	254*
	Th	E_X (keV)	11.119	11.210	11.236	11.289	11.348
		ΔE_X (eV)	0	91	117	170	229
		$\Delta' E_X$(eV)	0	87	123	174	225
$L\alpha_1$	Ta	E_X (keV)	8.146	8.232	8.264	8.319	8.354
L_3M_5		ΔE_X (eV)	0	86	118	173	208
		$\Delta' E_X$(eV)	0	84	118	166	214
	Au	E_X (keV)	9.713	9.800	9.824	9.876	
		ΔE_X (eV)	0	87	111	163	
		$\Delta' E_X$(eV)	0	82	115	163	209*
	Th	E_X (keV)	12.969	13.050	13.076	13.113	13.156
		ΔE_X (eV)	0	81	107	144	187
		$\Delta' E_X$(eV)	0	75	105	147	188

Table 1 (continued)

Line	Elem.	E_{Kr} (MeV/nucl)	0	0.6	1.2	2.4	4
		U (atomic units)	0	4.918	6.955	9.836	12.698
$L\beta_2$	Ta	E_X (keV)	9.652	9.846	10.070	10.244	10.370
L_3N_5		ΔE_X (eV)	0	294	418	592	718
		$\Delta' E_X$(eV)	0	289	407	574	740
	Au	E_X (keV)	11.585	11.873	11.992	12.131	
		ΔE_X (eV)	0	288	407	546	
		$\Delta' E_X$(eV)	0	280	395	558	720*
	Th	E_X (keV)	15.624	15.908	16.017	16.132	16.331
		ΔE_X (eV)	0	284	393	508	707
		$\Delta' E_X$(eV)	0	270	382	540	695
$L\beta_1$	Ta	E_X (keV)	9.343	9.438	9.454	9.509	9.552
L_2M_4		ΔE_X (eV)	0	95	111	166	209
		$\Delta' E_X$(eV)	0	84	117	164	211
	Au	E_X (keV)	11.442	11.522	11.542	11.601	
		ΔE_X (eV)	0	80	100	159	
		$\Delta' E_X$(eV)	0	78	110	155	201*
	Th	E_X (keV)	16.202		16.320	16.336	16.406
		ΔE_X (eV)	0		118	134	204
		$\Delta' E_X$(eV)	0	76*	108	152	196
$L\beta_3$	Ta	E_X (keV)	9.488	9.602	9.629	9.697	9.750
L_1M_3		ΔE_X (eV)	0	114	141	209	262
		$\Delta' E_X$(eV)	0	105	147	206	265
	Au	E_X (keV)	11.610	11.714	11.764	11.796	
		ΔE_X (eV)	0	104	154	186	
		$\Delta' E_X$(eV)	0	101	141	197	253*
	Th	E_X (keV)	16.426		16.545	16.570	16.630
		ΔE_X (eV)	0		119	144	204
		$\Delta' E_X$(eV)	0	79*	112	158	204

Table 1 (continued)

Line	Elem.	E_{Kr} (MeV/nucl)	0	0.6	1.2	2.4	4
		U (atomic units)	0	4.918	6.955	9.836	12.698
$L\beta_4$	Ta	E_X (keV)	9.212	9.309	9 339	9.394	9.457
L_1M_2		ΔE_X (eV)	0	97	127	182	245
		$\Delta' E_X$(eV)	0	93	132	186	241
	Au	E_X (keV)	11.205	11.297	11.338	11.386	
		ΔE_X (eV)	0	92	133	181	
		$\Delta' E_X$(eV)	0	92	130	185	236*
	Th	E_X (keV)	15.643		15.743	15.824	15.855
		ΔE_X (eV)	0		100	181	212
		$\Delta' E_X$(eV)	0	81*	116	166	215
$L\gamma_1$	Ta	E_X (keV)	10.895	11.220	11.301	11.482	11.646
L_2N_4		ΔE_X (eV)	0	325	406	587	751
		$\Delta' E_X$(eV)	0	299	418	587	755
	Au	E_X (keV)	13.382	13.697	13.803	13.950	
		ΔE_X (eV)	0	315	421	568	
		$\Delta' E_X$(eV)	0	296	415	582	748*
	Th	E_X (keV)	18.983		19.391	19.529	19.684
		ΔE_X (eV)	0		408	546	701
		$\Delta' E_X$(eV)	0	278*	391	550	708
$L\gamma_{2,3}$	Ta	E_X (keV)	11.248	11.584	11.612	11.860	11.940
$L_1N_{2,3}$		ΔE_X (eV)	0	336	364	612	692
		$\Delta' E_X$(eV)	0	292	405	565	723
	Au	E_X (keV)	13.759	14.087	14.216	14.329	
		ΔE_X (eV)	0	328	457	570	
		$\Delta' E_X$(eV)	0	309	429	599	769*
	Th	E_X (keV)	19.406		19.837	20.031	20.170
		ΔE_X (eV)	0		431	625	764
		$\Delta' E_X$(eV)	0	305*	430	605	780

Table 1 (continued)

Line	Elem.	E_{Kr} (MeV/nucl)	0	0.6	1.2	2.4	4
		U (atomic units)	0	4.918	6.955	9.836	12.698
$L\gamma_{4',4}$	Ta	E_X (keV)	11.641	12.220	12.329		
$L_1O_{2,3}$		ΔE_X (eV)	0	579	688		
		$\Delta' E_X$(eV)	0	521	729	1024*	1317*
	Au	E_X (keV)	14.290	14.890	15.074	15.243	
		ΔE_X (eV)	0	600	784	953	
		$\Delta' E_X$(eV)	0	532	732	1015	1296*
	Th	E_X (keV)	20.267		20.330		21.446
		ΔE_X (eV)	0		63		1179
		$\Delta' E_X$(eV)	0	267*	450	709*	971

Table 2 - Coefficients of the linear regression $E_X = a + bU$

Line	Element	Diagram line[6] (keV)	a	b	r^2
Ll	Ta	7.173	7.175	0.02104	0.998
	Au	8.494	8.496	0.01961	0.993
	Th	11.118	11.119	0.01775	0.997
$L\alpha_1$	Ta	8.146	8.148	0.01664	0.997
	Au	9.713	9.715	0.01639	0.997
	Th	12.969	12.970	0.01479	0.997
$L\beta_2$	Ta	9.652	9.656	0.05795	0.998
	Au	11.585	11.585	0.05674	0.999
	Th	15.624	15.629	0.05422	0.995
$L\beta_1$	Ta	9.343	9.347	0.01629	0.993
	Au	11.442	11.441	0.01579	0.991
	Th	16.202	16.203	0.01537	0.977
$L\beta_3$	Ta	9.488	9.492	0.02056	0.996
	Au	11.610	11.615	0.01947	0.983
	Th	16.426	16.426	0.01606	0.987
$L\beta_4$	Ta	9.212	9.211	0.01900	0.998
	Au	11.205	11.206	0.01854	0.983
	Th	15.643	15.639	0.01724	0.981
$L\gamma_1$	Ta	10.895	10.899	0.05924	0.998
	Au	13.382	13.386	0.05890	0.997
	Th	18.983	18.986	0.05560	0.999

Table2 (continued)

Line	Element	Diagram line[6] (keV)	a	b	r^2
$L\gamma_{2,3}$	Ta	11.248	11.267	0.05546	0.976
	Au	13.759	13.777	0.05913	0.987
	Th	19.406	19.411	0.05610	0.998
$L\gamma_{4',4}$	Ta	11.641	11.658	0.1024	0.980
	Au	14.290	14.339	0.0982	0.985
	Th	20.267	20.092	0.0899	0.743

Table 3 : Estimation of the electron vacancy configurations in Ta. The energy shifts taken in account are the calculated values $\Delta'E_X$ from table 1. Asteriskes indicate extrapolated or interpolated values (see text). Shifts in parentheses for M vacancies are estimated as described in the text. Shifts for N vacancies are estimated from values extracted from table 6.

line	E (MeV/n)	$\Delta'E_X$ (eV)	n_M	ΔE_M[14] (eV)	Diff. (eV)	n_N	ΔE_N (eV)	rest (eV)
Ll	0.6	105	2	57	48	7	42	6
L_3M_1	1.2	148	3	87	61	9	54	7
	2.4	209	5	148	61	9	54	7
						10	60	1
	4.0	269	6	184	85	13	78	7
						14	84	1
$L\alpha_1$	0.6	84	2	43	41	7	35	6
L_3M_5	1.2	118	3	65	53	9	45	8
	2.4	166	5	110	56	9	45	11
						10	50	6
	4.0	214	6	137	77	13	65	12
						14	70	7
$L\beta_2$	0.6	289	2	(115)	174	7	161	13
L_3N_5	1.2	407	3	(177)	230	9	207	23
	2.4	574	5	(304)	270	9	207	63
						10	240	30
	4.0	740	6	(374)	366	13	299	67
						14	322	44
$L\beta_1$	0.6	84	2	48	36	7	35	1
L_2M_4	1.2	117	3	72	45	9	45	0
	2.4	164	5	122	42	9	45	-3
						10	50	- 8
	4.0	211	6	145	66	13	65	1
						14	70	-4

Table 3 (continued)

line	E (MeV/n)	$\Delta' E_X$ (eV)	n_M	ΔE_M[14] (eV)	Diff. (eV)	n_N	ΔE_N (eV)	rest (eV)
$L\gamma_1$	0.6	299	2	125	174	7	168	6
L_2N_4	1.2	418	3	188	230	9	216	14
	2.4	587	5	317	270	9	216	54
						10	240	30
	4.0	755	6	382	373	13	312	61
						14	336	37
$L\beta_3$	0.6	105	2	(55)	50			
L_1M_3	1.2	147	3	(84)	63			
	2.4	206	5	(146)	60			
	4.0	265	6	(176)	89			
$L\beta_4$	0.6	93	2	(47)	46			
L_1M_2	1.2	132	3	(73)	59			
	2.4	186	5	(128)	58			
	4.0	241	6	(154)	87			
$L\gamma_{2,3}$	0.6	292	2	116	176	7	161	15
$L_1N_{2,3}$	1.2	405	3	175	230	9	207	23
	2.4	565	5	297	268	9	207	61
						10	230	38
	4.0	723	6	363	360	13	299	61
						14	322	38
$L\gamma_{4',4}$	0.6	521	2	143	378			
$L_1O_{2,3}$	1.2	729	3	219	510			
	2.4	1024*	5	372	652			
	4.0	1317*	6	456	861			

Table 4 : Estimation of the electron vacancy configurations in Au. The energy shifts taken in account are the calculated values $\Delta'E_X$ from table 1. Asteriskes indicate extrapolated or interpolated values (see text). Shifts in parentheses for M vacancies are estimated as described in the text. Shifts for N vacancies are estimated from values extracted from table 6.

line	E (MeV/n)	$\Delta'E_X$ (eV)	n_M	ΔE_M[14] (eV)	Diff. (eV)	n_N	ΔE_N (eV)	rest (eV)
Ll	0.6	102	2	63	39	5	32	7
L_3M_1	1.2	142	3	96	46	6	38	8
	2.4	198	4	128	70	9	58	12
						10	64	6
	4.0	254*	5	162	92	12	77	15
						13	83	9
$L\alpha_1$	0.6	82	2	47	35	5	27	7
L_3M_5	1.2	115	3	71	44	6	32	12
	2.4	163	4	96	67	9	49	18
						10	54	13
	4.0	209*	5	121	88	12	65	23
						13	70	18
$L\beta_2$	0.6	280	2	(130)	150	5	125	25
L_3N_5	1.2	395	3	(197)	198	6	150	48
	2.4	558	4	(264)	294	9	225	69
						10	250	44
	4.0	720*	5	(332)	388	12	300	88
						13	325	63
$L\beta_1$	0.6	78	2	53	25	5	27	-2
L_2M_4	1.2	110	3	79	31	6	32	-1
	2.4	155	4	106	48	9	49	-1
						10	54	-6
	4.0	201*	5	134	67	12	65	2
						13	70	-3

Table 4(continued)

line	E (MeV/n)	$\Delta' E_X$ (eV)	n_M	ΔE_M[14] (eV)	Diff. (eV)	n_N	ΔE_N (eV)	rest (eV)
$L\gamma_1$	0.6	296	2	138	156	5	133	23
L_2N_4	1.2	415	3	209	206	6	159	47
	2.4	582	4	280	300	9	243	57
						10	265	35
	4.0	748*	5	353	369	12	324	45
						13	345	24
$L\beta_3$	0.6	101	2	(70)	31			
L_1M_3	1.2	141	3	(103)	38			
	2.4	197	4	(139)	58			
	4.0	253*	5	(176)	77			
$L\beta_4$	0.6	92	2	(68)	24			
L_1M_2	1.2	130	3	(98)	32			
	2.4	185	4	(130)	55			
	4.0	236*	5	(162)	74			
$L\gamma_{2,3}$	0.6	309	2	130	179			
$L_1N_{2,3}$	1.2	429	3	197	232			
	2.4	599	4	264	335			
	4	769*	5	333	436			
$L\gamma_{4',4}$	0.6	532	2	163	369			
$L_1O_{2,3}$	1.2	732	3	248	484			
	2.4	1015	4	333	682			
	4.0	1296*	5	420	876			

Table 5 : Estimation of the electron vacancy configurations in Th. The energy shifts taken in account are the calculated values $\Delta'E_X$ from table 1. Asteriskes indicate extrapolated or interpolated values (see text). Shifts in parentheses for M vacancies are estimated as described in the text. Shifts for N vacancies are estimated from values extracted from table 6.

line	E (MeV/n)	$\Delta'E_X$ (eV)	n_M	ΔE_M[14] (eV)	Diff. (eV)	n_N	ΔE_N (eV)	rest (eV)
Ll	0.6	87	1	36	51	6	42	9
L_3M_1	1.2	123	2	73	50	7	49	1
	2.4	174	3	109	65	9	63	2
	4.0	225	4	147	78	11	77	1
$L\alpha_1$	0.6	75	1	29	46	6	36	10
L_3M_5	1.2	105	2	58	47	7	42	5
	2.4	147	3	86	61	9	54	7
	4.0	188	4	116	72	11	66	6
$L\beta_2$	0.6	270	1	(78)	192	6	180	12
L_3N_5	1.2	382	2	(158)	234	7	210	24
	2.4	540	3	(238)	302	9	270	32
	4.0	695	4	(321)	374	11	330	44
$L\beta_1$	0.6	76*	1	30	46	6	36	10
L_2M_4	1.2	108	2	63	45	7	42	3
	2.4	152	3	93	59	9	54	5
	4.0	196	4	125	71	11	66	5
$L\gamma_1$	0.6	278*	1	83	195	6	186	9
L_2N_4	1.2	391	2	169	222	7	217	5
	2.4	550	3	253	297	9	279	18
	4.0	708	4	338	370	11	341	29

Table 5 (continued)

line	E (MeV/n)	$\Delta' E_X$ (eV)	n_M	ΔE_M[14] (eV)	Diff. (eV)	n_N	ΔE_N (eV)	rest (eV)
$L\beta_3$	0.6	79*	1	(41)	38			
L_1M_3	1.2	112	2	(86)	26			
	2.4	158	3	(125)	33			
	4.0	204	4	(168)	36			
$L\beta_4$	0.6	81*	1	(32)	49			
L_1M_2	1.2	116	2	(68)	48			
	2.4	166	3	(100)	66			
	4.0	215	4	(129)	86			
$L\gamma_{2,3}$	0.6	305*	1	78	227	6	180	47
$L_1N_{2,3}$	1.2	430	2	158	272	7	210	62
	2.4	605	3	238	367	9	270	97
	4.0	780	4	321	459	11	330	129

Table 6 : Estimation of the mean energy shifts per M vacancy (eV) of $L\beta_2$, $L\beta_3$ and $L\beta_4$ lines.

Line	$L\beta_2$	$L\beta_3$	$L\beta_3$[15]	$L\beta_4$	$L\beta_4$[15]
Ta	60	29	42	25	38
Au	66	35	47	33	42
Th	79	42	56	33	48

Table 7 : Estimation of the mean energy shifts per N vacancy (eV) of various L X-ray lines . The accuracy is within 10%.

Line	Ll	$L\alpha$	$L\beta_2$	$L\beta_1$	$L\gamma_1$	$L\gamma_{2,3}$
Ta	6	5	23	5	24	23
Au	6.4	5.4	25	5.4	27	
Th	7	6	30	6	31	30

Table 8 : Most probable vacancy configurations in Ta, Au and Th targets corresponding to 0.6 to 4.0 MeV/nucleon Kr beams, as deduced from the present measurements.

	Number of M vacancies				Number of N vacancies			
E(MeV/n)	0.6	1.2	2.4	4.0	0.6	1.2	2.4	4.0
Ta	2	3	5	6	7	9	9 - 10	13 - 14
Au	2	3	4	5	5	6	9 - 10	12 - 13
Th	1	2	3	4	6	6 - 7	8 - 9	10 - 11

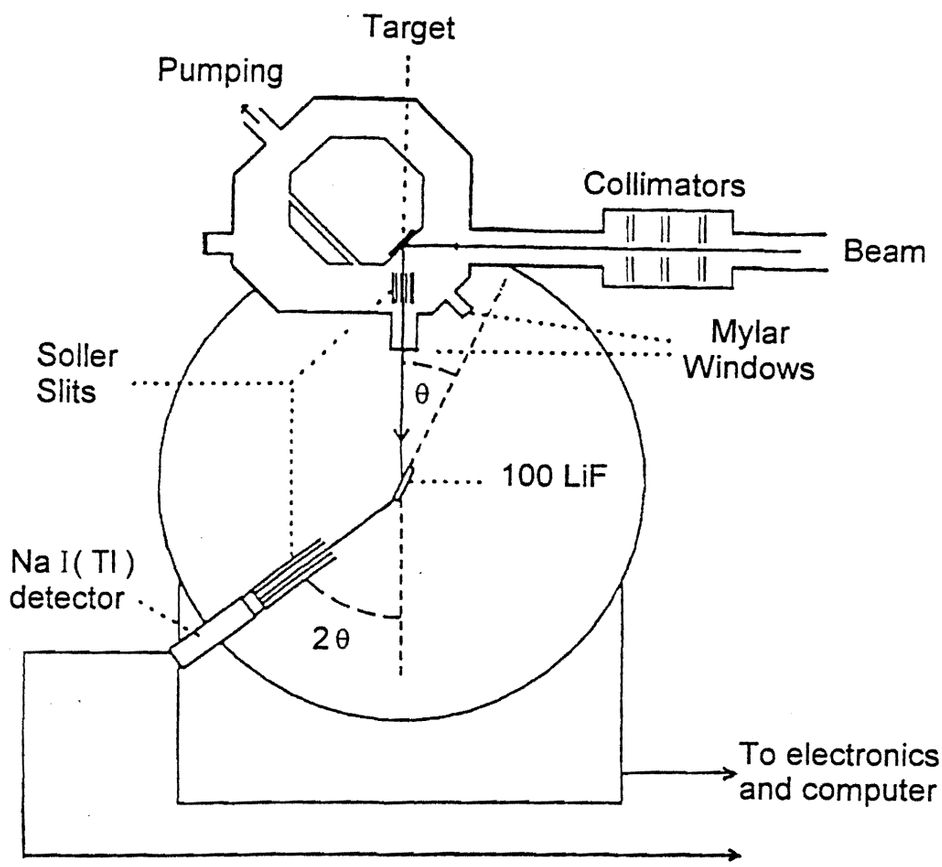

Figure 1 Schematic view of the experimental setup.

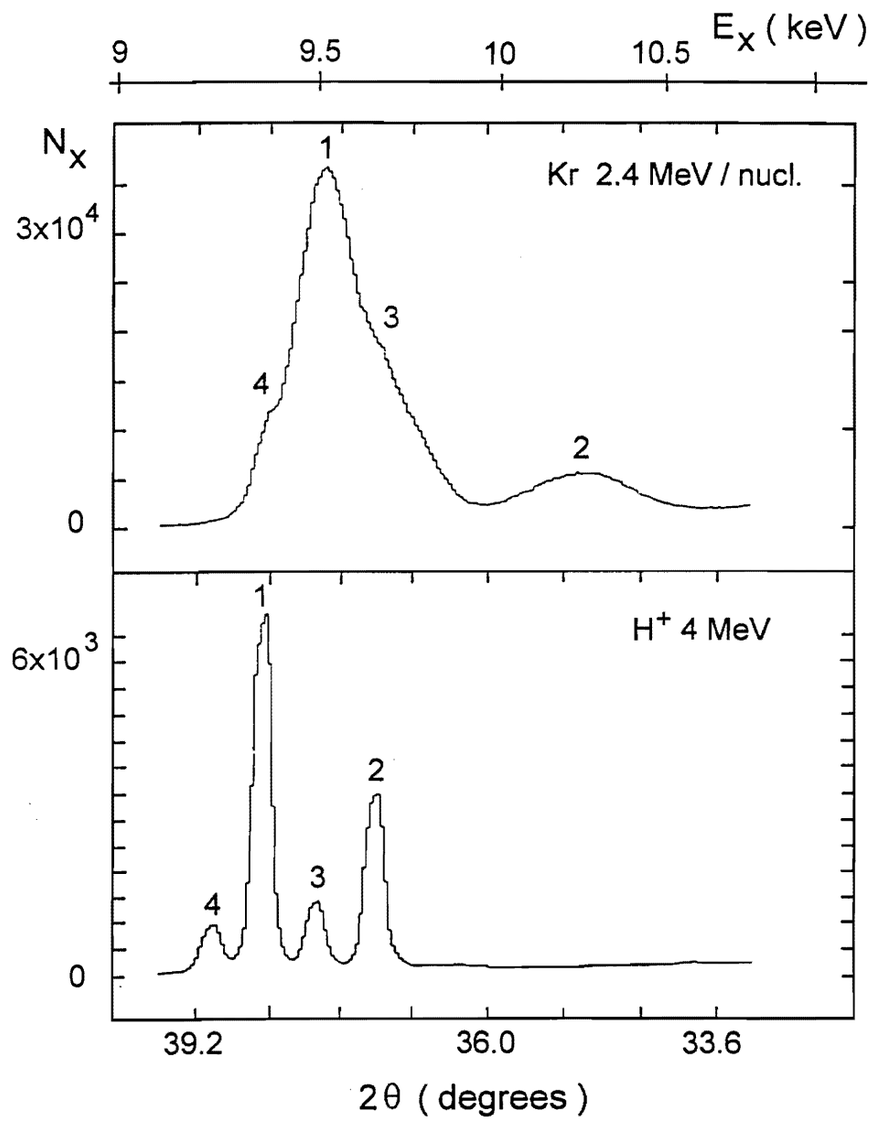

Figure 2 Ta Lβ spectra induced by a 2.4 MeV/nucleon Kr beam and by 4 MeV protons

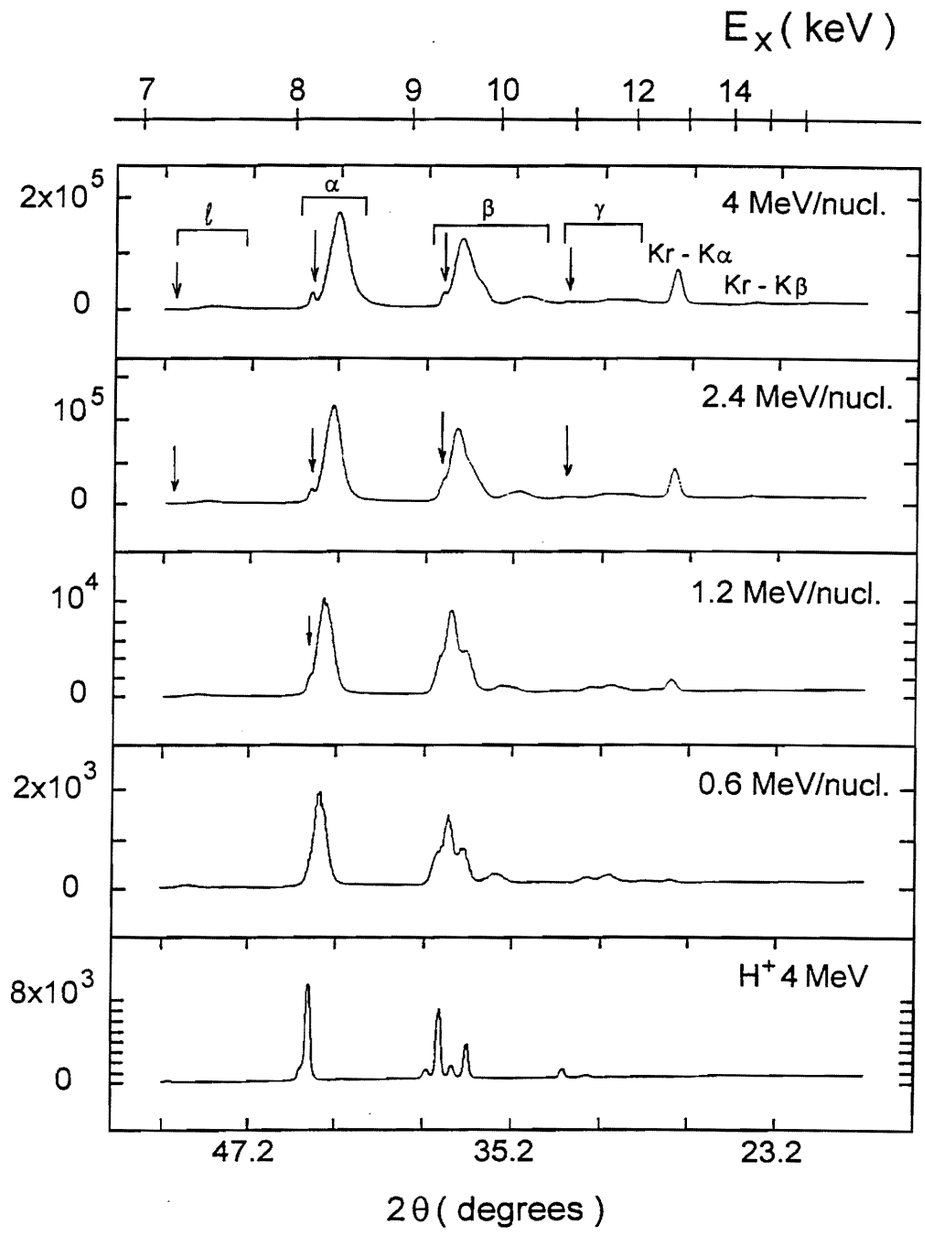

Figure 3 Ta L X-ray spectra induced by 4 MeV protons and 0.6 to 4 MeV/nucleon Kr beams. Diagram lines are indicated by arrows as they appear in the spectra.

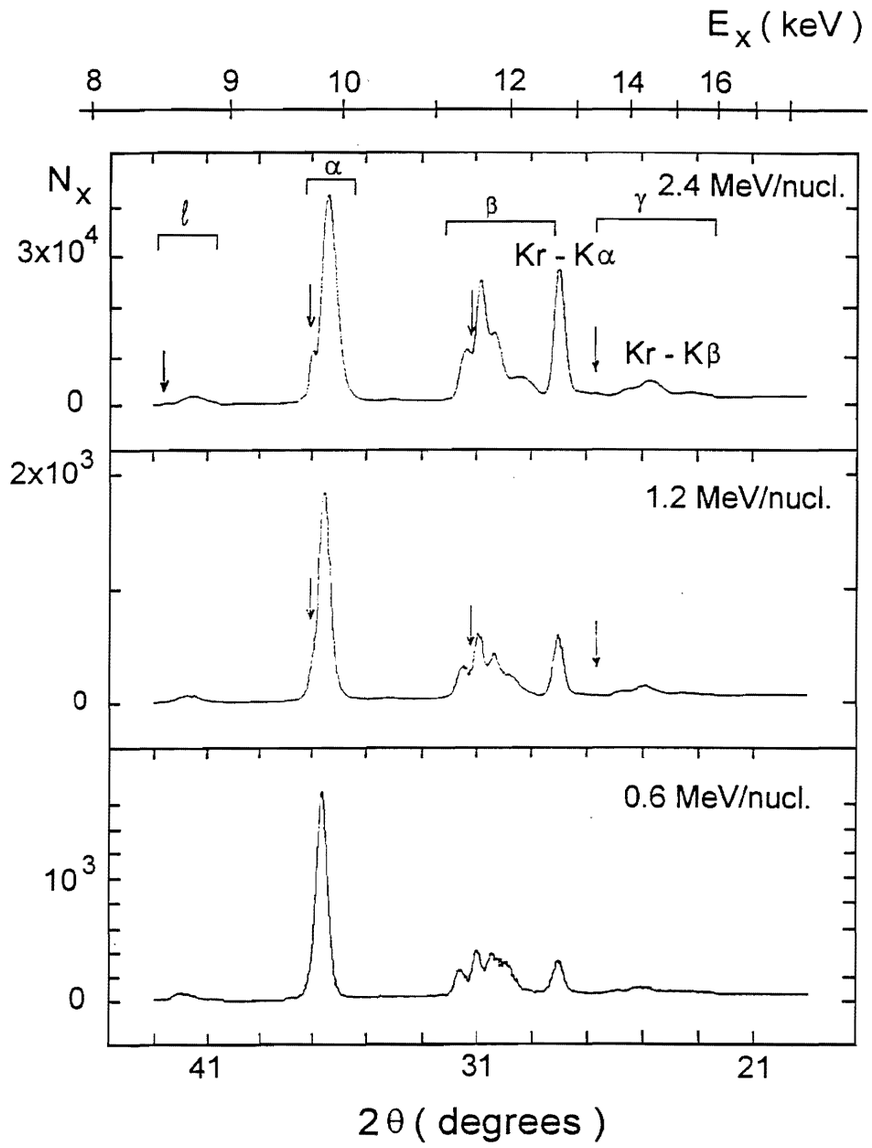

Figure 4 Au L X-ray spectra induced by 0.6 to 4 MeV/nucleon Kr beams. Diagram lines are indicated by arrows as they appear in the spectra.

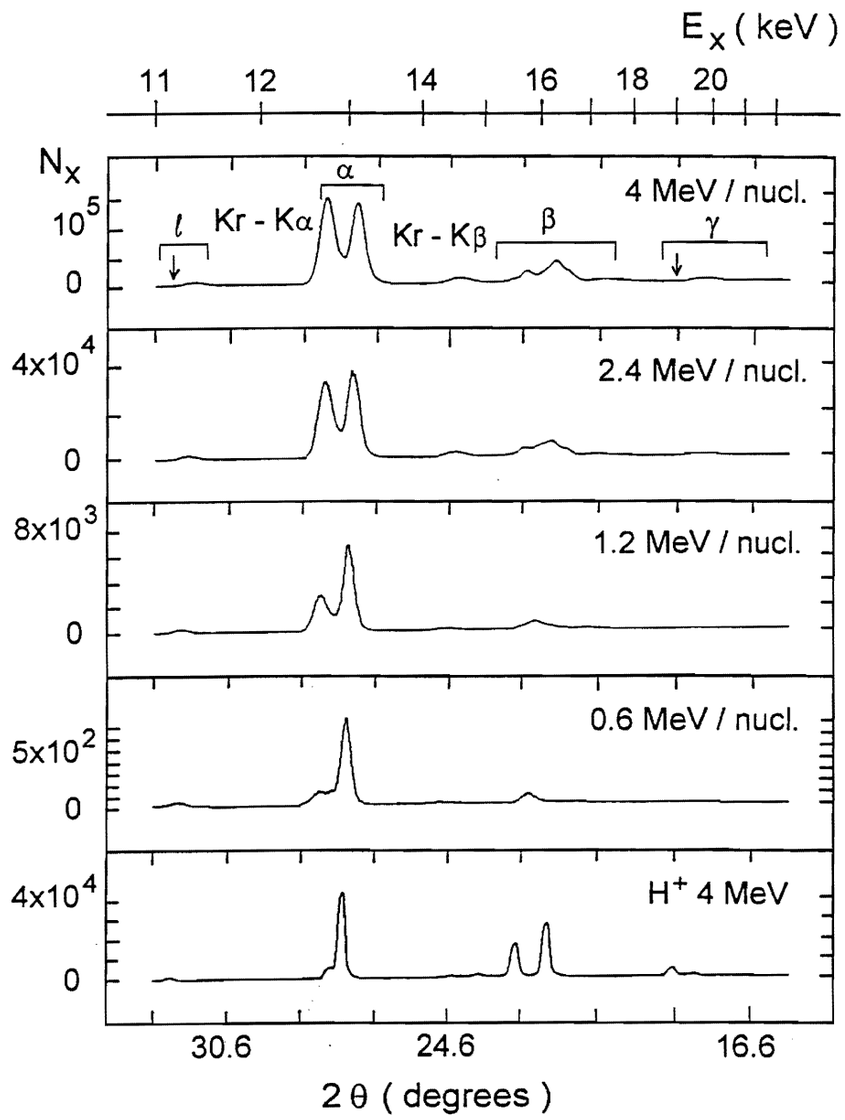

Figure 5 Th L X-ray spectra induced by 4 MeV protons and 0.6 to 4 MeV/nucleon Kr beams. Diagram lines are indicated by arrows as they appear in the spectra.

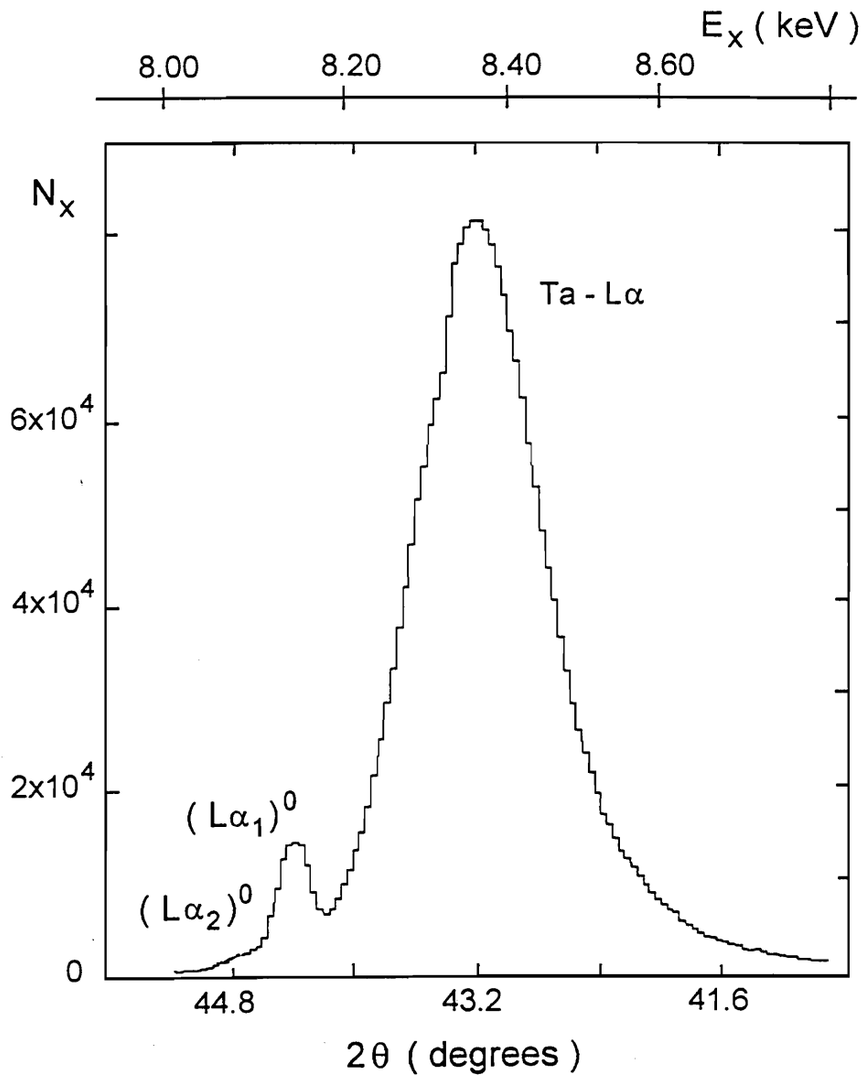

Figure 6 Ta Lα line induced by 4 MeV/nucleon Kr ions showing the $(L\alpha_1)^0$ and $(L\alpha_2)^0$ diagram lines

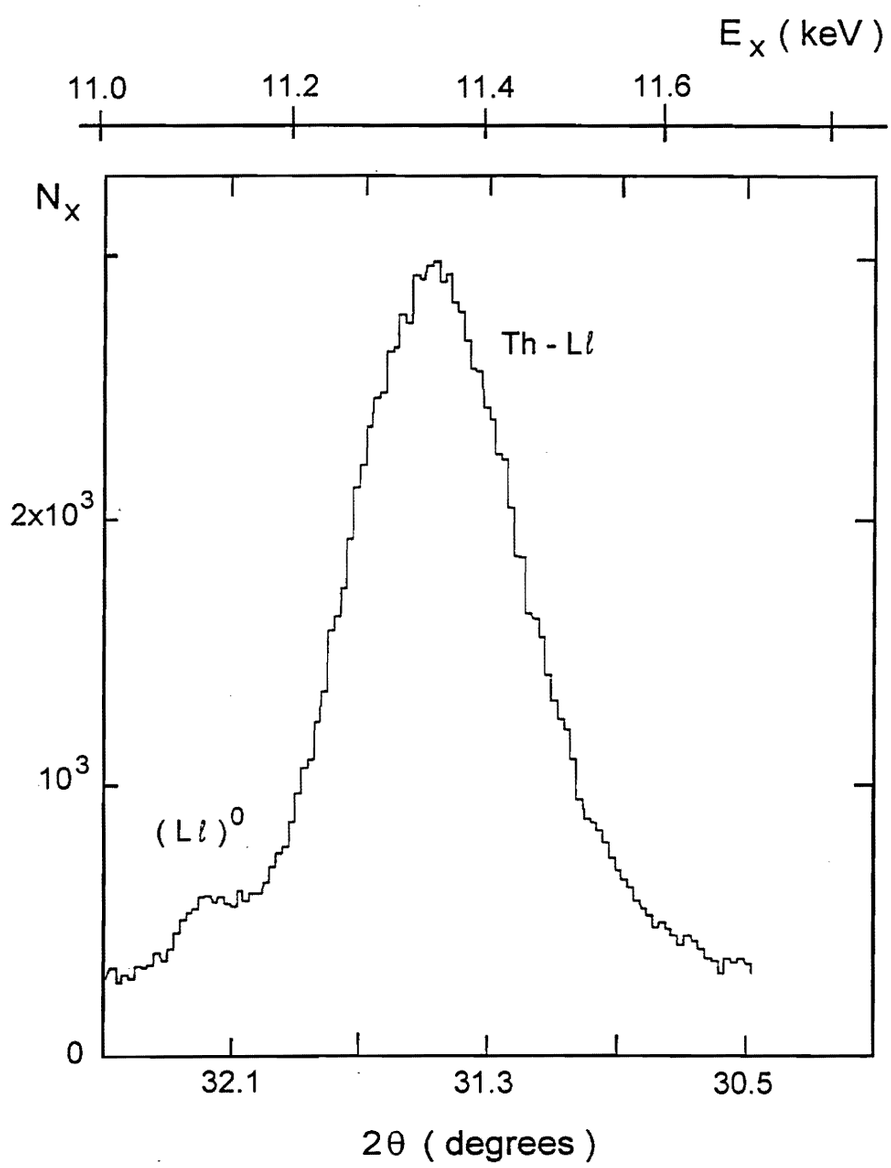

Figure 7 Th L*l* line induced by 4 MeV/nucleon Kr ions showing the $(L\ell)^0$ diagram line.

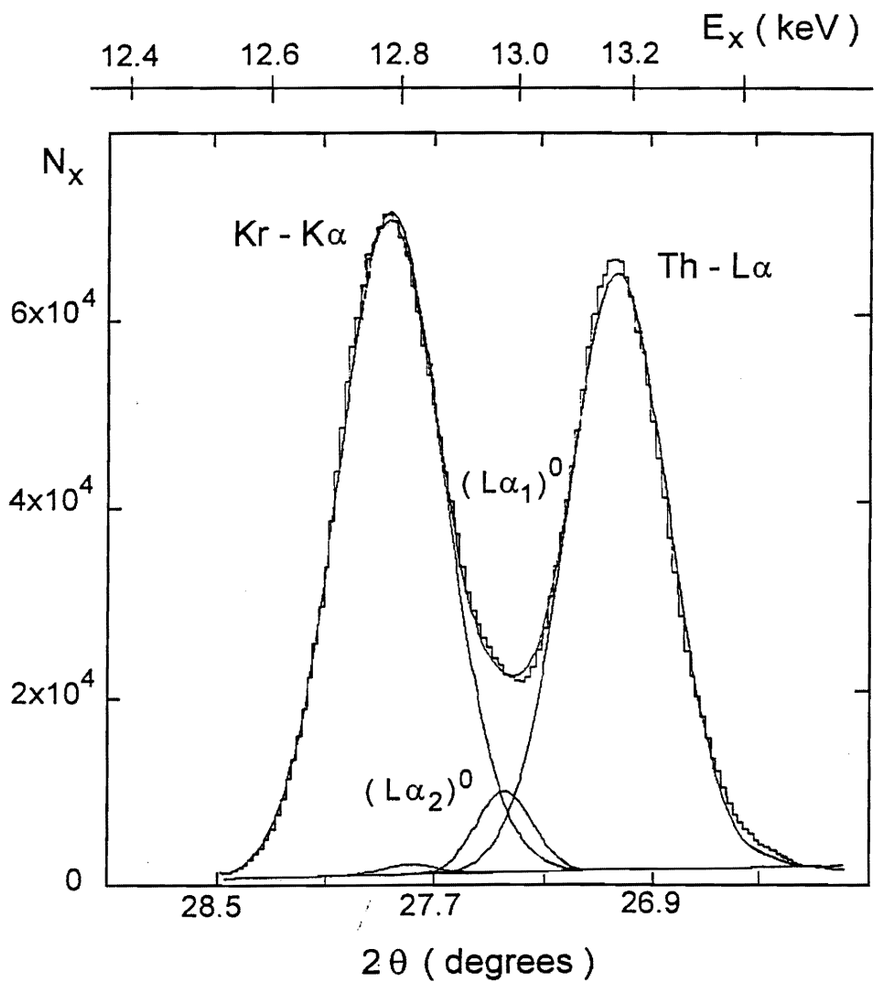

Figure 8 Deconvolution of the Kr Kα and Th Lα peaks induced by 4 MeV/nucleon Kr ions.

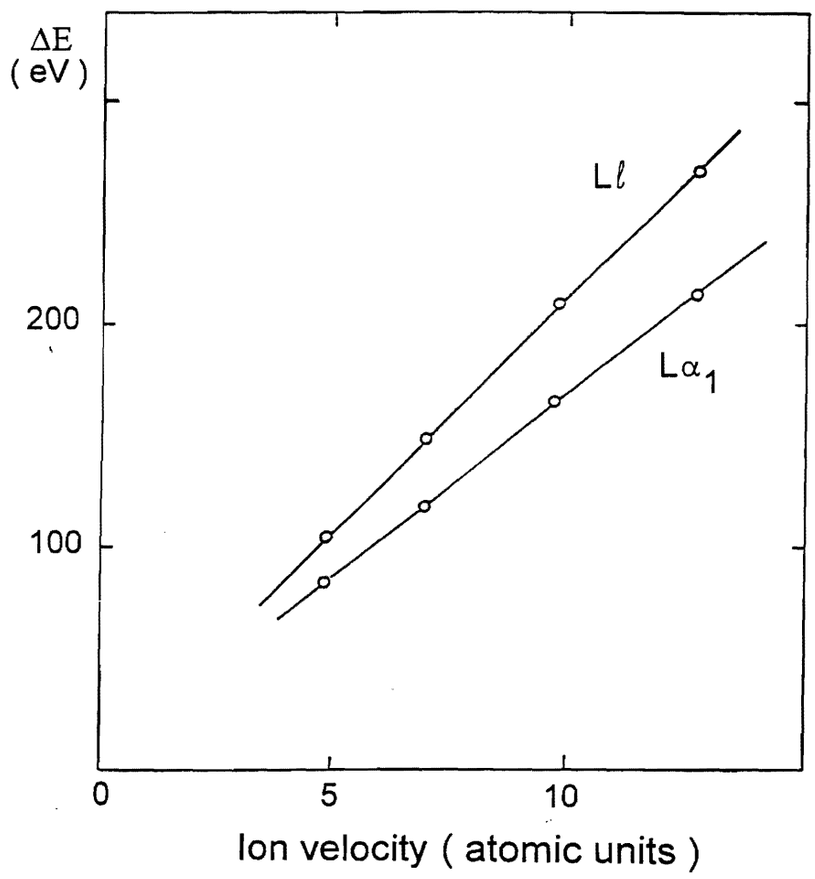

Figure 9 Energy shift of the peak centroids of the Ta L*l* and $L\alpha_1$ lines as a function of the Kr beam velocity V(atomic units).

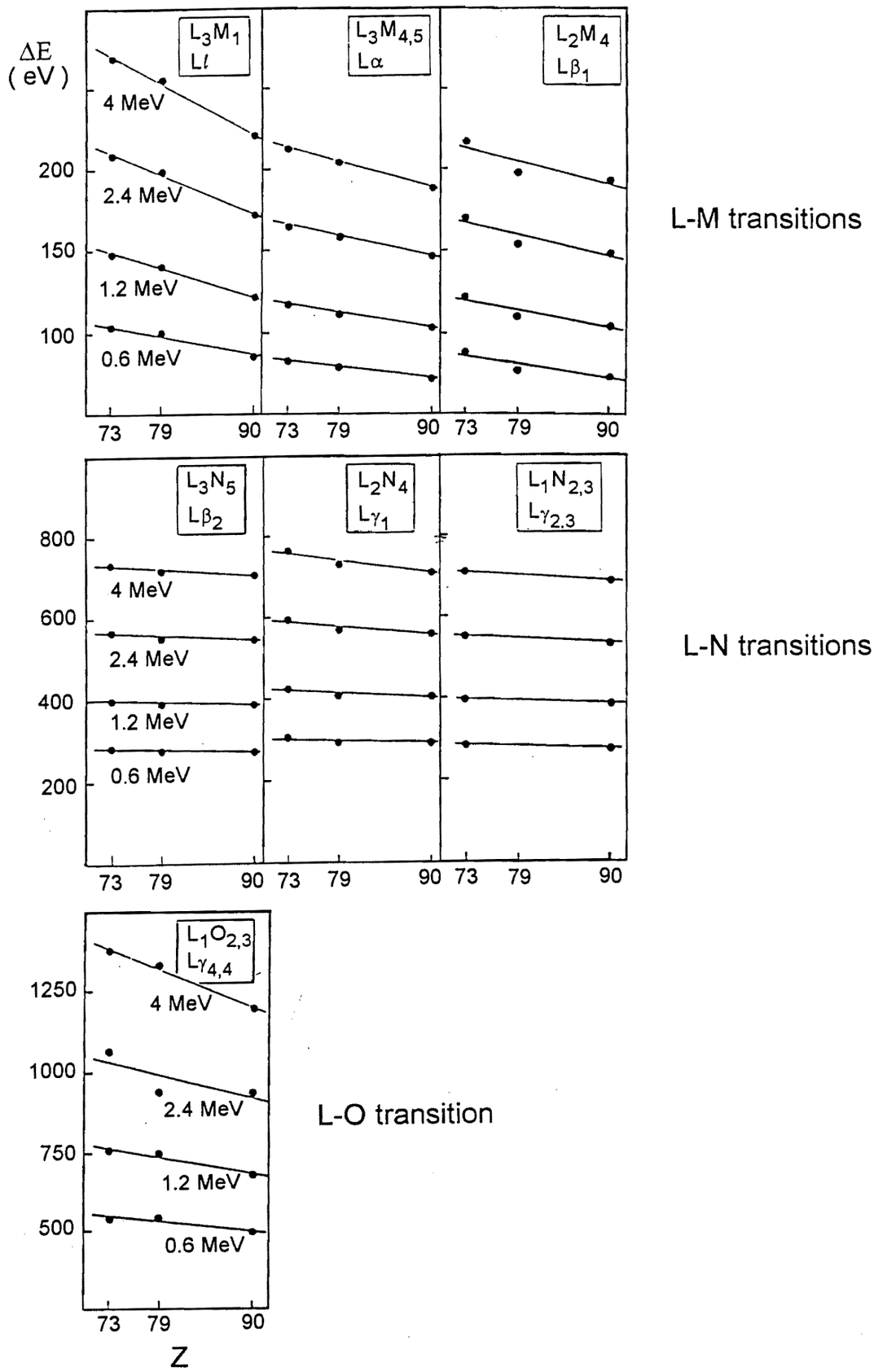

Figure 10 Energy shifts of the peak centroids of Ta, Au and Th lines as a function of the target atomic number for the various incident energies.

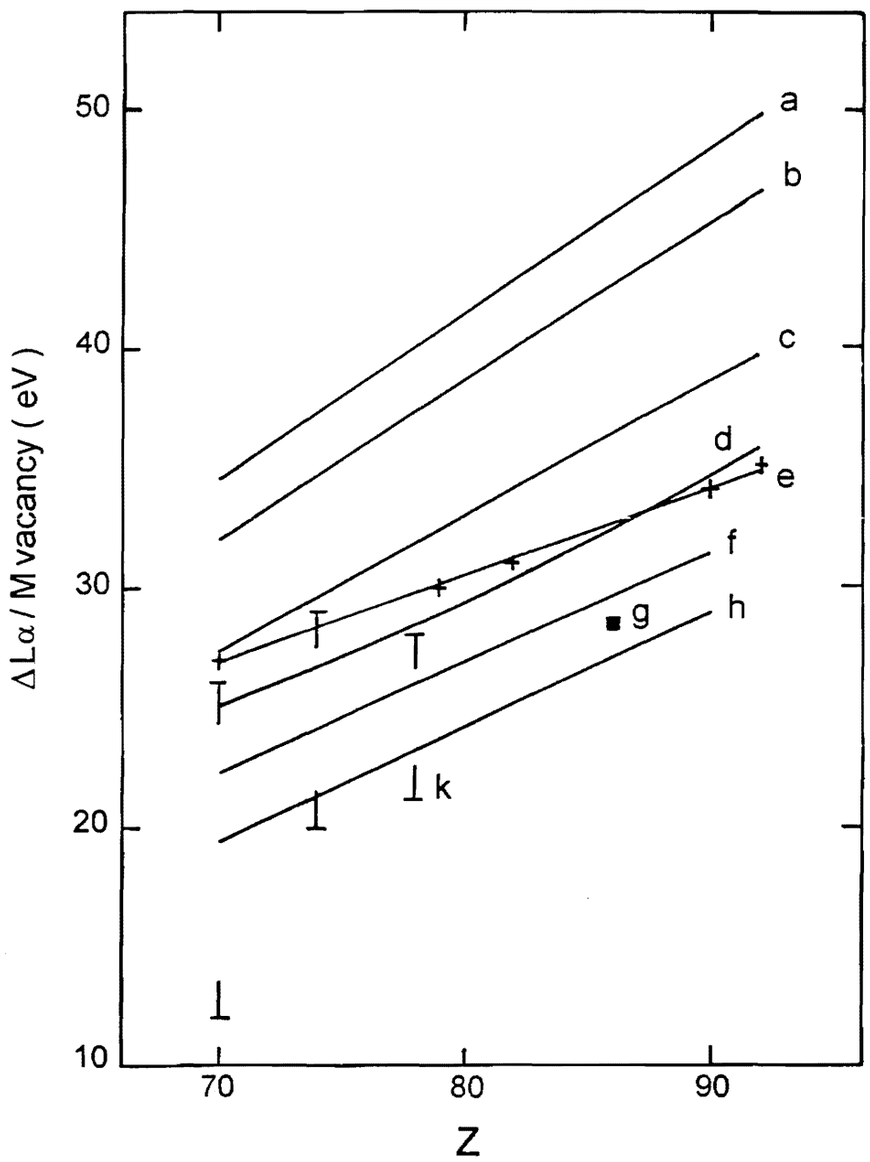

Figure 11 Mean energy shifts per M vacancy from different authors for the Lα line as a function of the target atomic number (Z) :
a) Values deduced from Zschornack *et al.* [15], b) Shift for the first M vacancy[15], c) Values of Burch *et al.* [9], d) Values of Parente *et al.* [11 and17], e) Values of Hagmann [10], f) Mean values given by Uchai *et al.* [14], g)Calculation of Roy *et al.* [13], h) Shift for the first M vacancy [14]. k) Limits given by Rao *et al.*[12].